Available online at www.sciencedirect.com

ScienceDirect

Advances in Space Research 77 (2026) 8406–8418

ADVANCES IN SPACE RESEARCH (a COSPAR publication)

www.elsevier.com/locate/asr

Very high energy proton acceleration in Vela-type pulsar wind nebulae

A.M. Bykov *, A.N. Fursov, K.P. Levenfish *, A.E. Petrov

Ioffe Institute, Saint-Petersburg, Polytechnicheskaya Str., 26, 194021, Russia

Received 1 June 2025; received in revised form 12 August 2025; accepted 19 August 2025
Available online 22 August 2025

Abstract

High-quality measurements of cosmic ray (CR) fluxes have revealed a number of features in the spectra of protons, leptons, and nuclei. These can be due to contributions of nearby CR accelerators over the CR sea produced by the galactic supernova remnants. Pulsars, their relativistic winds, and their bright synchrotron nebulae are among the candidate sources of CRs. The structure of two powerful pulsar wind nebulae (PWNe) created by the pulsars Crab and Vela is studied with arcsecond resolution by Chandra X-ray Observatory. We constructed a numerical relativistic ideal MHD model of PWNe which reproduces the observed X-ray morphology of the Vela nebula, a prototype of nebulae with a double X-ray torus. The spatial and temporal resolution of the simulated MHD flows with frozen-in magnetic fields allowed us to study the confinement and acceleration of multi-TeV cosmic ray protons in nebulae belonging to the class of double-torus objects. We directly solved the equation of motion for individual CR particles injected from the central part of the PWN and propagating through the simulated MHD flows. It is shown that very high energy protons can be confined within a double-torus nebula and accelerated to sub-PeV energies in its shear flows associated with regular large-scale vortices. The model treats the CR protons as test particles and therefore may be considered as the minimal model of CR acceleration in double-torus type PWNe.

Keywords: Pulsar wind nebulae; MHD modeling; Cosmic rays

1. Introduction

The origin of most of cosmic ray (CR) protons in the energy range from tens of GeV to hundreds of TeV is attributed to supernova remnants (see e.g. Amato, 2014). Diffusive acceleration by supernova shock waves via the Fermi mechanism can provide efficient CR acceleration consistent with high-quality multiwavelength observations of supernova remnants in the Galaxy (e.g. Blandford and Eichler, 1987; Malkov and Drury, 2001; Bykov et al., 2018; Marcowith et al., 2020). Still, other types of galactic sources of high energy protons may contribute at least to the locally observed CR fluxes. Recent precision observations have revealed interesting features in the cosmic rays spectra of both hadrons and leptons. Some of these can be understood as contributions from local CR accelerators. The CR bump between 0.5 and 50 TeV can be produced by nuclei accelerated at the bow shocks of nearby stars (Malkov and Moskalenko, 2021). The increase in the fraction of positrons above a few GeV, detected by PAMELA and AMS-02 magnetic spectrometers, may be due to leptons accelerated at the bow shock observed in the nebula of the nearby millisecond pulsar PSR J0437–4715 (Bykov et al., 2019). To adequately interpret these and other features of cosmic ray fluxes measured with high precision, detailed modeling of accelerators of various types is required. In this study, we focus on pulsar wind nebulae.

* Corresponding authors.
E-mail addresses: byk@astro.ioffe.ru (A.M. Bykov), a.n.fursov@mail.ioffe.ru (A.N. Fursov), ksen@astro.ioffe.ru (K.P. Levenfish), a.e.petrov@mail.ioffe.ru (A.E. Petrov).

https://doi.org/10.1016/j.asr.2025.08.046

Rotation powered pulsars and magnetars are among the most energetic objects, with power comparable to that of supernova ejecta. They are considered among the likely sources of CRs in the PeV regime (Bell, 1992; Bell and Lucek, 1996; Berezhko, 1994; Arons, 2003; Bednarek and Bartosik, 2004; Arons, 2012; Bykov et al., 2024). Winds from rapidly rotating, highly magnetized neutron stars-pulsars arise as relativistic outflow of highly magnetized plasma with a frozen-in magnetic field. The composition of the winds is a long-standing problem. The establishment of the synchrotron nature of the broadband emission from the Crab Nebula and successful models of the multiwavelength emission from pulsar magnetospheres and nebulae left no doubt that the winds are dominated by electron–positron pairs. Although sub-PeV observations of pulsar wind nebulae are consistent with purely leptonic winds (see, e.g. Amato and Olmi, 2021), the presence of ions in the winds is still a matter of debate. Cao et al. (2021) detected PeV gamma-rays from Crab Nebula, which, according to the authors, can be explained by the leptonic model. Meanwhile, the hadron model can also account for the PeV radiation. The First LHAASO Catalog of Gamma-Ray Sources (Cao et al., 2024) lists more than 15 PWNe powered by pulsars with spin-down luminosity above 10^{35} erg s^{-1}. A few dozens of TeV radiating PWNe is listed in the H.E.S.S. Galactic Plane Survey (Abdalla et al., 2018).

Like primary electrons, ions can also be extracted from the surface of neutron stars. A number of particle-in-cell (PIC) simulations conducted in recent decades have examined particle acceleration in the pulsar magnetosphere and shown that the presence of an ion component can lead to important effects. Hardening of pair spectra due to more efficient acceleration of positrons (Amato and Arons, 2006), production of sub-PeV protons by millisecond pulsars (Guépin et al., 2020), and enrichment of ultra-high-energy cosmic rays with (sub) PeV nuclei (Kotera et al., 2015) are some of the possible consequences. Philippov and Spitkovsky (2018) found that the acceleration efficiency to the highest energies (which may be close to PeV) appears to be higher for low-inclination pulsars.

Pulsar wind nebulae (PWNe) are known to be efficient particle accelerators. The Crab Nebula converts about 25 % of the pulsar's spin-down luminosity into a broadband non-thermal luminosity produced by synchrotron emission from accelerated leptons (Arons, 2012). The external environment actively participates in the formation of the structure of PWNe, thereby influencing their acceleration efficiency. This efficiency can be increased in the presence of a strong external flow, especially a supersonic one, since non-thermal particles can gain additional energy in the region where this flow collides with the pulsar wind. Bykov et al. (2017) showed that in supersonic PWNe, even with a weak bow shock as seen in Vela, colliding flows can produce very hard spectra since most of their energy taken by particles is transferred to particles with the highest achievable energies.

The structure of MHD flows not only determines the acceleration efficiency of nebulae, but also shapes their X-ray appearance. This opens the way to a detailed study of this structure by direct comparison of high-resolution X-ray images of a nebula with synchrotron X-ray maps calculated on top of its numerical relativistic MHD (RMHD) model. The very first numerical models of the Crab Nebula (Komissarov and Lyubarsky, 2004; Del Zanna et al., 2004) showed that the MHD structure is sensitive to many parameters of the system comprising the wind, the pulsar and their external environment. The observer's viewing angle is added to these parameters, when it comes to X-ray morphology. The Crab and Vela nebulae, prototypes of objects with single-torus and double-torus X-ray morphology, coincidentally appear at almost the same viewing angle. This became clear immediately after their observation by the Chandra X-ray telescope (Weisskopf et al., 2000; Helfand et al., 2001; Pavlov et al., 2001). Since then, many suggestions were made in the literature about which parameter is responsible for their different appearance in X-rays (e.g, Helfand et al., 2001; Pavlov et al., 2001; Kargaltsev et al., 2015; Reynolds et al., 2017, to name just a few). Given the nonlinearity and complexity of the system, only numerical modeling (MHD and, to some extent, PIC) may allow one to determine the most realistic of these suggestions.

In most MHD simulations of compact PWNe with jet-torus X-ray morphology, as seen in Crab and Vela, the external matter is modeled as supernova ejecta in spherically symmetric expansion. A more realistic approach would be to consider this matter in relative motion with respect to the nebula, since pulsars have proper motion and SNRs often enter into non-spherically symmetric expansion due to the density gradient in their surroundings. Recently, an MHD model implementing this approach has been proposed. Adding an extra degree of freedom allowed the model to describe X-ray features of the Crab Nebula that previous models had difficulty with (e.g., an inner ring with uniform brightness, a sprite, asymmetric jets, diffuse counter-jet, etc.; Levenfish et al., 2021). In addition, the model was able to reproduce virtually all known X-ray features in the Vela Nebula (Ponomaryov et al., 2019; Ponomaryov et al., 2020; Ponomaryov et al., 2021; Ponomaryov et al., 2023; Fateeva et al., 2023; Petrov et al., 2023) and to predict the existence of previously unknown features, the presence of which in Vela has been recently confirmed by reanalysis of the Chandra observations (Levenfish et al., 2025). Last but not least, the model showed that the X-ray appearance of the nebula is drastically different for observers looking at it from the windward and leeward sides, even if both observers' line of sight makes the same angle to the pulsar's rotation axis (Levenfish et al., 2021).

With such a MHD model in hand, one can study the acceleration efficiency of PWNe by injecting populations of pre-accelerated protons into the nebula and tracking their evolution in space and energy due to interaction with background MHD flows. It is clear that each nebula has its own unique flow pattern, and yet in PWNe of the same type it is generally quite similar, suggesting similarities in the mechanisms and trajectories of particle acceleration.

In this study, we will focus on double-torus-type nebulae. Their well-known representative is Vela. This nebula is inflated by a powerful nearby pulsar located at 295 pc from Earth. This certainly makes the Vela Nebula an interesting potential local source of CR protons. The spin-down luminosity of its pulsar, which is almost entirely spent on creating the pulsar wind, is close to 10^{37} erg s^{-1}. Although the characteristic age of the pulsar is about 11,000 years, its currently observed nebula is much younger: it is probably only 2–3 thousand years old (Mattana et al., 2011). The pulsar re-inflated it when its former relic nebula was crushed by one-sided interaction with the supernova's reverse shock. The passage of the shock wave initiated a fast directed flow of ejecta in the vicinity of the pulsar, with which the newly formed nebula is still interacting. This external flow moves almost counter to the pulsar's proper motion and appears supersonic in the pulsar's rest frame. Because it is only slightly supersonic, it does not destroy the jet-torus structure of the newly formed nebula, but still forces it to form a weak bow shock (the outlines of which can be guessed at in Fig. 1 in Chevalier and Reynolds, 2011).

According to our MHD model, for the nebula to acquire the double-torus X-ray morphology observed in Vela, it must encounter a strong external flow moving at near-sonic or slightly supersonic speed relative to the pulsar. Under the influence of such a flow, pulsars with a low magnetized wind and a high magnetic inclination can radically restructure their nebulae. This is due to the fact that the combination of the above-mentioned parameters (slightly supersonic flow + weakly magnetized wind + high magnetic inclination) greatly contributes to stabilization of the wind termination shock, which is a necessary condition for the existence of a double-torus. Once the shock wave stabilizes in size and geometry, the nebular flows lose their usual stochasticity and become quasi-laminar. This allows them to form regular large-scale MHD structures with a highly ordered magnetic field. The field is completely dominated by the toroidal component, which has been recently confirmed by Vela observations with the magnetic polarimeter IXPE (Xie et al., 2022).

Reynolds et al. (2017) surmised that the rarity of double-torus objects among jet-torus-type PWNe may be due to the rare combination of conditions required for their formation. Indeed, the need for a strong but not too strong external flow (combined with a large magnetic inclination and a weakly magnetized wind) makes the appearance of a double torus in PWNe a rather rare phenomenon. When the flow no longer meets the above condition, a double torus gradually transforms into a single one. In this sense, the double torus can arise both temporarily and permanently. Within an evolving supernova remnant, a double torus can form temporarily, either after the reverse shock passes over the pulsar or when the pulsar crosses a region of the remnant where the velocity difference between the ejecta and the pulsar approaches or slightly exceeds the local speed of sound (see e.g. van der Swaluw et al., 2003). In the interstellar medium, a double torus can persist as long as the pulsar is capable of inflating the nebula, provided that the pulsar has a low proper velocity, slightly exceeding the speed of sound in the (stationary) medium.

Depending on the cases described right above, regular large-scale MHD structures of a light-year scale can persist in double-torus objects for several hundred to several tens of thousands of years. The combination of size and lifetime of these structures makes them suitable for efficient accelerating multi-TeV protons (with gyroradii of the order of sub-light-year scale), and the magnitude of their magnetic fields ($\sim$ 5–30 μG in our Vela-type model) allows them to confine such protons throughout their acceleration. These features may place double-torus PWNe in line with other sources of (sub) PeV protons, which is of interest for cosmic ray physics and PeV astronomy.

To study the production of (sub) PeV protons in the double-torus PWNe we performed RMHD-PIC simulations of MHD structures and proton acceleration in these objects. The paper is organized as follows. Sect. 2 describes the structures of the double-torus nebulae, and Sect. 3 presents the trajectories of protons accelerated in these structures. In Sect. 4 we discuss the efficiency of particle acceleration and the populations formed by accelerated protons. In Sect. 5 we draw conclusions from our simulations. A detailed description of the RMHD-PIC setup is given in the appendices.

2. Structure of MHD flows in double-torus X-ray nebulae

A recently proposed MHD model of compact X-ray nebulae has shown that they can acquire a *regular* double-torus X-ray morphology if the working surface of their wind termination shock is stabilized (Ponomaryov et al., 2019; Ponomaryov et al., 2021; Ponomaryov et al., 2023). This means that the working surface must constantly maintain smooth outlines and should not experience sudden changes in size. Stabilization of the shock requires a combination of several conditions. Modeling within the *ideal* MHD framework allowed to reveal at least three of them. The pulsar should: (1) move with transonic or slightly supersonic speed relative to the external environment; (2) have a low magnetized wind; (3) have a large magnetic inclination (the angle between its rotational and magnetic axes).

When these conditions are met, a characteristic pattern of MHD flows develops in the nebula (Fig. 1). Its equator

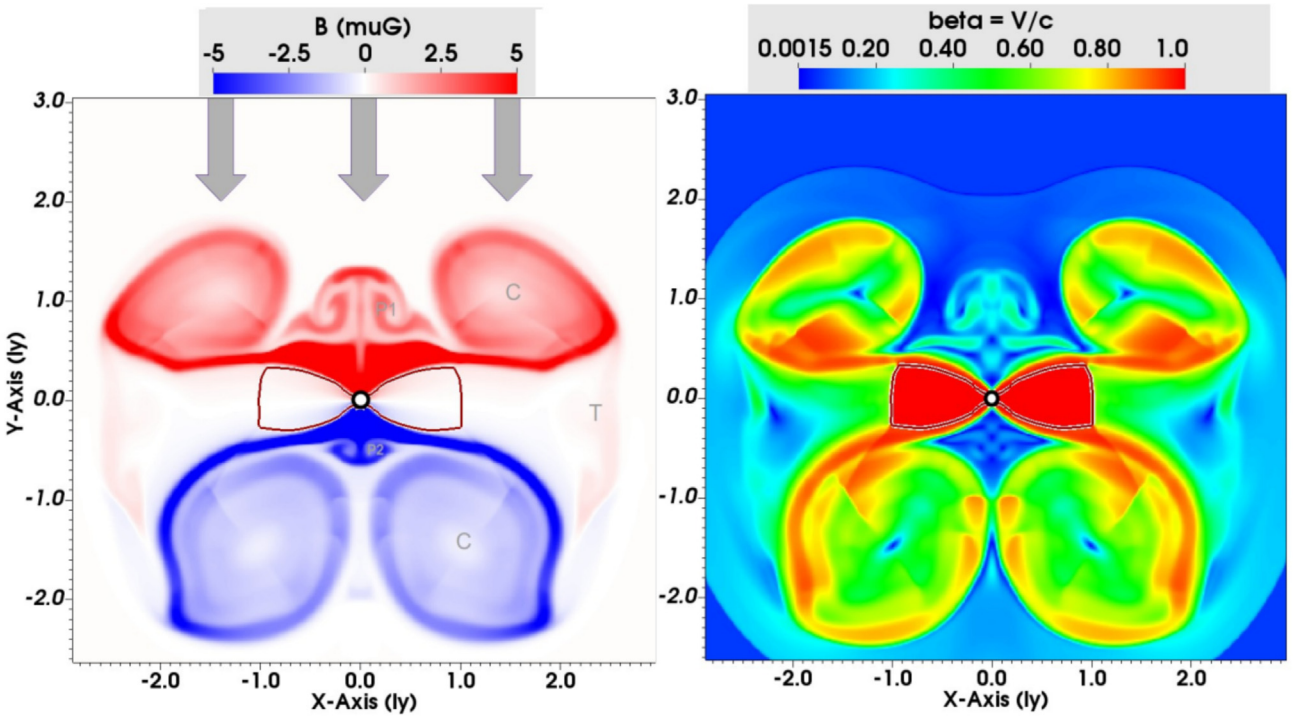

Fig. 1. Structure of RMHD flows in the model double-torus pulsar wind nebula. Shown are simulated maps of the azimuthal magnetic field (in μG, left) and the magnitude of the flow velocity (in units of the light velocity c, right). The pulsar location is marked with a white circle. Red contour outlines an approximate position of the pulsar wind termination shock. Red and blue color on the magnetic field map refer for different magnetic polarity. On the magnetic field map: gray arrows show the direction of the external flow in the reference frame associated with the pulsar; the letters marks individual MHD structures of the nebula: the circulation vortices (C), the tongue-like structures (T), the vortex near the polar axis in the windward hemisphere of the nebula (P1), and the recirculation vortex in the leeward funnel of the wind termination shock (P2). Note that the color scales are adjusted to highlight the structure of MHD flows and do not reflect the minimum and maximum values of B and β.

is occupied by a wide, slow, barely magnetized flow, the plasma in which remains in an overcompressed and underexpanded state almost to the edges of the compact X-ray nebula. On both sides, the equatorial flow touches upon highly magnetized, relativistic, narrow-channel flows running almost parallel to the equatorial plane. Highly magnetized flows originate in hemispheres with different magnetic polarity and form immediately downstream of the arched vaults of the wind termination shock. They can communicate with each other, but not directly (as happens in the single-torus PWNe), but through the mediation of the overcompressed equatorial flow (Petrov et al., 2023), which keeps them separated from each other throughout their entire length.

Highly magnetized flows generate and feed two regular large-scale circulation vortices with toroidal geometry (marked with 'C" in the left panel in Fig. 1), which form at the middle latitudes of the nebula in its neighboring hemispheres. The combination of two strongly magnetized toroidal vortices and two highly magnetized relativistic flows separated by a barely magnetized equatorial flow gives the nebula the appearance of a double torus.

In fact, each highly magnetized narrow-channel flow splits into two parts as it approaches the edges of the compact nebula. One part rises to higher latitudes and forms a circulation vortex, the other turns toward the equator and stretches out into a long tongue of magnetic plasma (marked with "T" in the left panel in Fig. 1). All structures of the nebula are very regular and weakly dynamic, with the exception of the magnetic tongues. The latter are quite dynamic and can from time to time penetrate into the neighboring hemisphere of reverse magnetic polarity.

The external flow which is incident upon the nebula pushes its windward circulation vortex further from the polar axis and presses the leeward circulation closer to this axis. Due to the closure of the leeward vortex on the axis, a recirculation vortex (marked with "P2") develops in the lee funnel of the shock. This smaller scale vortex is also regular and has a toroidal geometry.

The structure of MHD flows is illustrated in Fig. 1, which shows a poloidal slice of a modeled nebula. The left and right panels show the instantaneous distributions of the azimuthal magnetic field (in μG) and the velocity of the RMHD flows (in units of the speed of light c). In both panels, the pulsar is indicated by a white circle at the origin, and the wind termination shock is outlined by a contour. The vertical arrows show the direction of a weakly supersonic (in the pulsar's rest frame) flow of external matter that the nebula encounters. Note that the spatial resolution of the presented model, chosen to be suitable for the acceleration of multi-TeV protons, turned out to be insufficient for the nebula to form thin polar outflows (jets). However,

in high-resolution double-torus models, such jets are confidently formed (see, e.g., Ponomaryov et al., 2023; Fateeva et al., 2023), although their role in particle acceleration has yet to be studied.

3. Trajectories of accelerating protons

Double-torus pulsar wind nebulae are characterized by quasi-laminar flows that carry a frozen-in magnetic field of highly ordered toroidal geometry. Flows of this kind tend to organize into regular large-scale MHD structures (patterns). In each hemisphere of the nebula, these structures are represented by a narrow-channel relativistic flow and a number of large-scale toroidal vortices (Fig. 1). The largest of these, called the *circulation vortex,* underlies the X-ray torus in the corresponding hemisphere. Smaller vortices typically occur near the polar axis of the nebula. All of these structures are formed by shear flows, and all of them can persist in the nebula as long as it retains the double-torus X-ray morphology.

The presence of regular large-scale vortices – closed circular patterns of MHD flows with a shear in field and velocity – allows the nebula to confine and accelerate nonthermal protons even in the absence of large-scale turbulence. The most productive and efficient acceleration engine in the nebula is its circulation vortex in the *windward* hemisphere (which is the upper in figures). This engine becomes especially efficient in combination with a narrow-channel flow. Figs. 2 and 3 illustrate how this engine operates.

Fig. 2 presents general views of trajectories created by two test-particle protons (A and B). Both protons are injected into the nebula at same location as the pulsar wind and then follow a similar path before being caught in the windward circulation. At first, the particles are advected by the narrow-channel flow along the arched vault of the wind termination shock, then successively surf two large-scale polar magnetic vortices and, after a series of scatterings between them and the main circulation vortex, are drawn into the latter.

During random scatterings, proton A (shown in the left panel) loses almost all the energy it acquired during the surf; the last scattering fling this proton into the outer strongly magnetized layers of the circulation vortex, almost parallel to its streamlines and down the flow. Proton B (in the right panel) manages to slightly increase the energy acquired in the surf, and the last reflection throws it through the outer layers of the circulation, across its streamlines. The difference in the energies and ways of entering the circulation leads to the fact that A and B protons stay in this vortex for different periods of time, and follow different trajectories. This, however, does not prevent them from gaining similar energy.

In Fig. 3 we show close-ups of the trajectories traces by protons A and B inside the circulation. Despite their impressively different appearance, these trajectories have

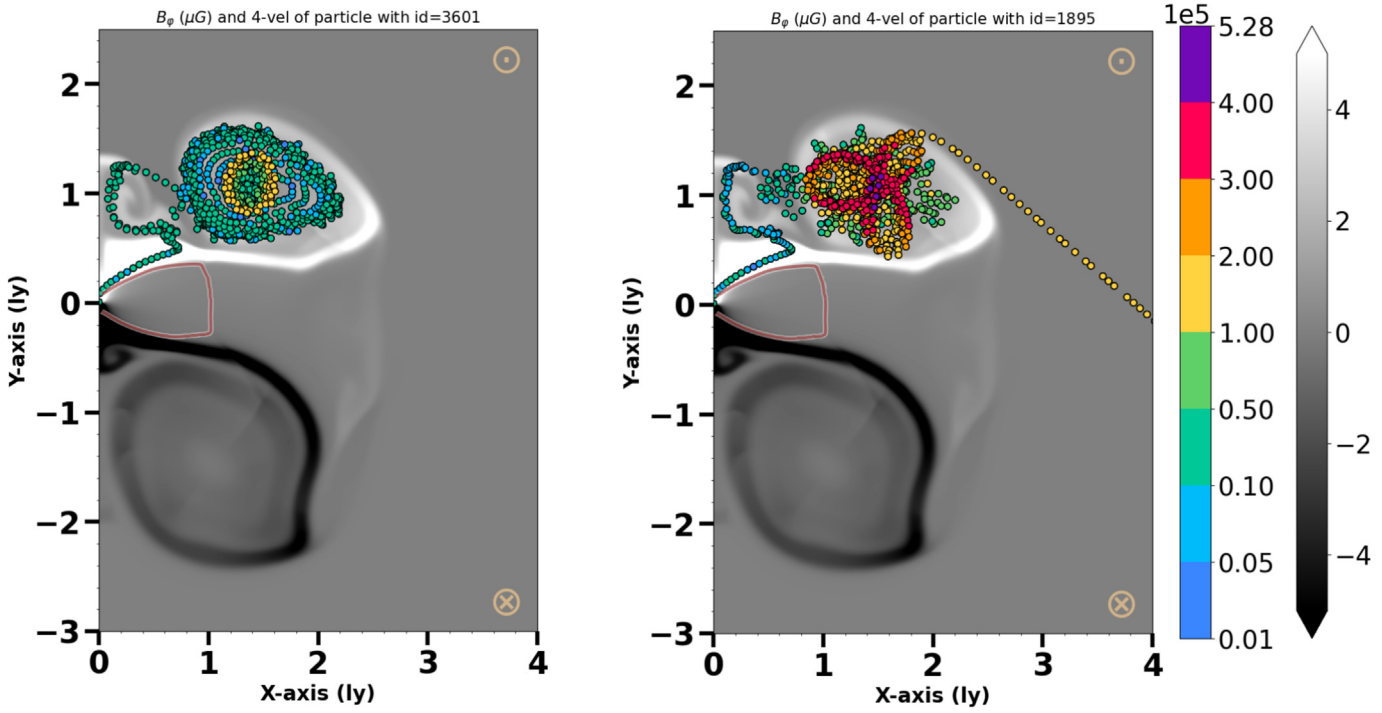

Fig. 2. Acceleration trajectories of two test-particle protons – A (left panel) and B (right panel) in a toroidal circulation vortex in the windward side of a double-torus pulsar wind nebula. In each panel bold dots show the positions of the proton at the set of consecutive time moments, the color of dots indicate the proton's 4-velocity according the colorbar on the right. The trajectories are superimposed onto a gray-color map of the PWN's azimuthal magnetic field.

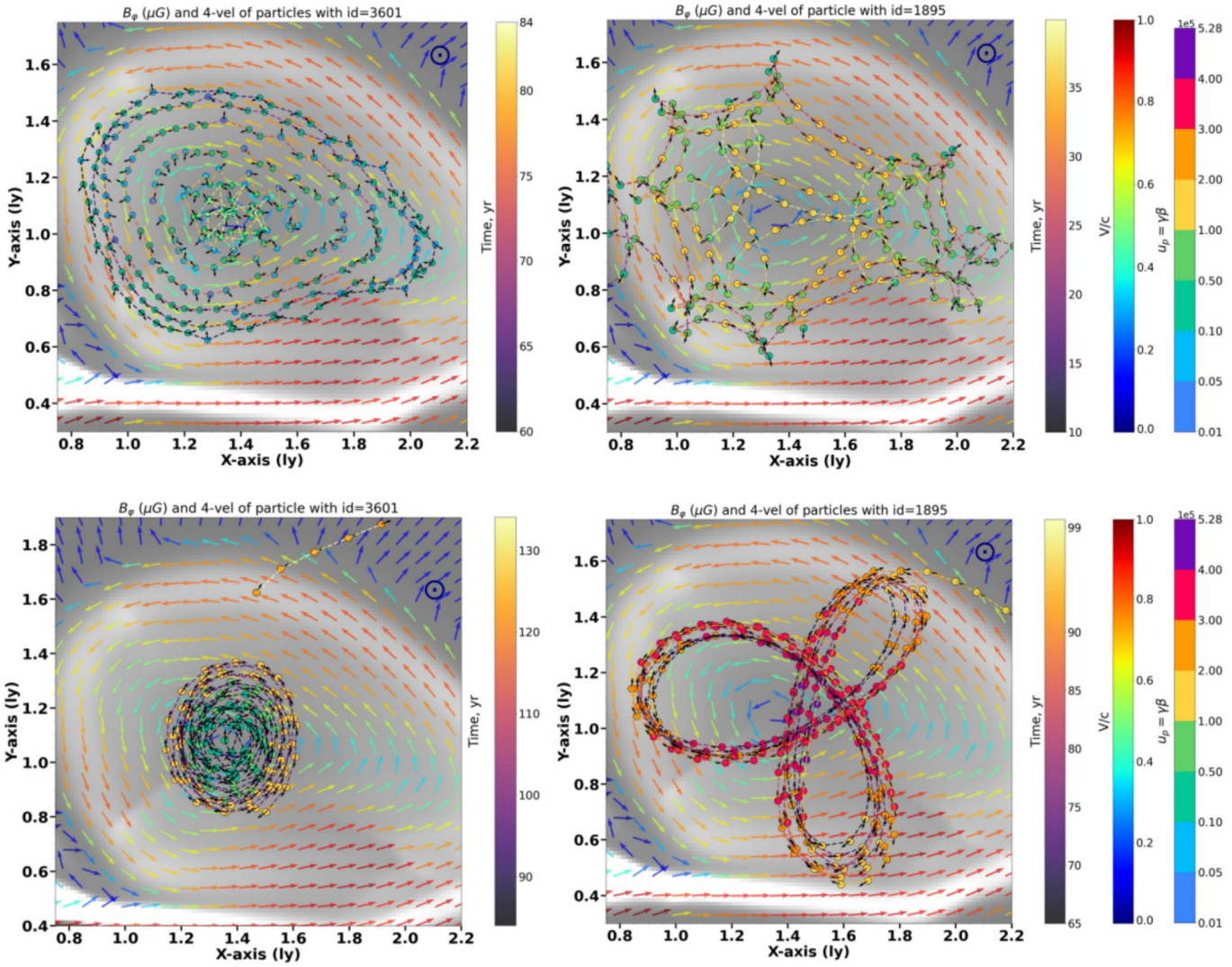

Fig. 3. Close-ups of the trajectories of two protons (A and B) shown in Fig. 2. The panels on the left are for proton A, and the panels on the right are for proton B. The upper panels (A1, B1) show a fragment of the initial part of the trajectory of the corresponding protons, and the lower panels (A2, B2) a fragment of the final part of this trajectory. The panel A2, in fact, shows two fragments: inside the vortex and at the exit from it (the trajectory between them is not shown, for clarity). Like in Fig. 2, the trajectories are superimposed on the gray-color map of the azimuthal magnetic field. The trajectories are shown simultaneously by (i) the color dots that show the positions of proton at the set of the consecutive moments of time, where the color shows the magnitude of the proton's 4-velocity (the rightmost colorbars) and black arrows its direction and (ii) the dashed lines along the trajectory whose color shows the time since the protons' injection (colorbars marked 'Time, yr'). Color arrows show the magnitude and direction of the simulated RMHD flows' velocity (middle colorbar marked 'V/c').

something in common. They can be divided into two physically different parts: the initial and the final, fragments of which we show in panels (A1, B1) and (A2, B2), respectively. In the initial part of the trajectories, protons A and B spiral toward the circulation eye, moving downstream on average. In the final part, both protons begin to move against the flow, gradually increasing their energy.

The time colorbar near panel A1 shows that it takes about 80 years for proton A to enter the acceleration process. Most of those years the particle spends in the vortex, being slowly advected downstream toward the vortex's eye (so that its trajectory follows an Archimedian spiral). As the particle spirals toward the eye, it finds itself in progressively weaker magnetic fields, so that its gyroradius R_g increases noticeably, even though its energy changes only slightly. Eventually, R_g becomes large enough for the particle to feel a shear in field and velocity, and it begins to scatter across the sheared flow. This draws the particle into the acceleration process, the details of which can be seen in panel A2, which shows a fragment of the acceleration trajectory. The latter also follows an Archimedean spiral, which unwinds so slowly that after 125 years the particle is still in the vortex.

The time colorbar near panel B1 shows that proton B begins to accelerate just 40 years after being injected into the nebula. For most of these years, it approaches the eye of the circulation along a trajectory resembling a kind of cycloid superimposed on an Archimedean spiral. Already

at this part of the trajectory one can notice that proton's energy undergoes quasi-periodic changes. It increases when the particle crosses the innermost layers of the circulation (where the velocity and field shears are strongest), and returns to almost the previous value when the particle returns to the outer layers (where the shifts are noticeably weaker, as follows from the corresponding colorbars). Similar changes in energy can be traced in the acceleration part of the trajectory shown in panel B2. Because of these quasi-periodic changes, an unusual phenomenon can be observed: for a long time a vortex can retain particles whose gyroradii are formally larger than the radius of the vortex itself. For instance, proton B quasi-periodically increases its Lorentz factor to $\sim 4.5 \cdot 10^5$ (to the energy of ~ 420 TeV), at which its gyroradius reaches 0.7 light years and becomes formally larger than the vortex radius of 0.6 light years. Another example of this curious phenomenon is given in Fig. 8.

The pattern of flows in double-torus nebulae allows nonthermal particles to accelerate not only in shear flows, but also in converging flows, as shown in Fig. 4. The latter mechanism becomes available due to the presence of large-scale vortices with opposite directions of rotation. Recall that all these vortices are actually toroids surrounding the polar axis of the nebula. Therefore, even flows in the same vortex, in a certain section of it, turn out to be counter-streaming if we consider them on different sides of the axis. As for different vortices with opposite directions of rotation, an example with them is shown in Fig. 5.

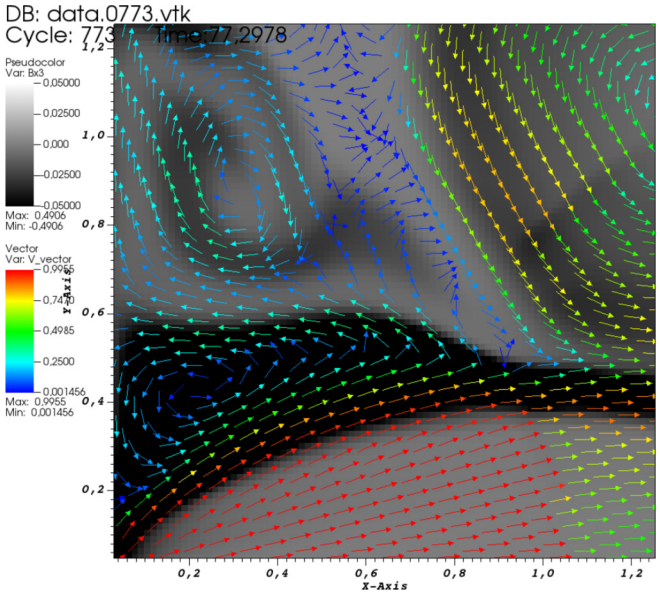

Fig. 5. Close-up of an area of converging flows from three regular large-scale toroidal vortices in the windward hemisphere of a double-torus nebula. Small arrows represent the velocity field of MHD flows. The color of the arrows indicates the magnitude of the local velocity according to the colorbar on the left. To guide the eye, the arrows are superimposed on a gray-color gradient map of the magnetic field of MHD flows. A general view of this region can be found in Fig. 1.

4. Populations of accelerated protons

How efficiently the pulsar wind nebulae can accelerate non-thermal protons and to what energies depends on a number of factors – where protons enter the nebula, what is the mechanism of their pre-acceleration, what is the energy of the pre-accelerated particles, to name just a few. All these questions are still being debated. Our simulations indicate that the efficiency of acceleration may depend even on the sign of magnetic polarity in the windward hemisphere of the nebula (Fig. 6). (This polarity reflects the polarity in the corresponding magnetic

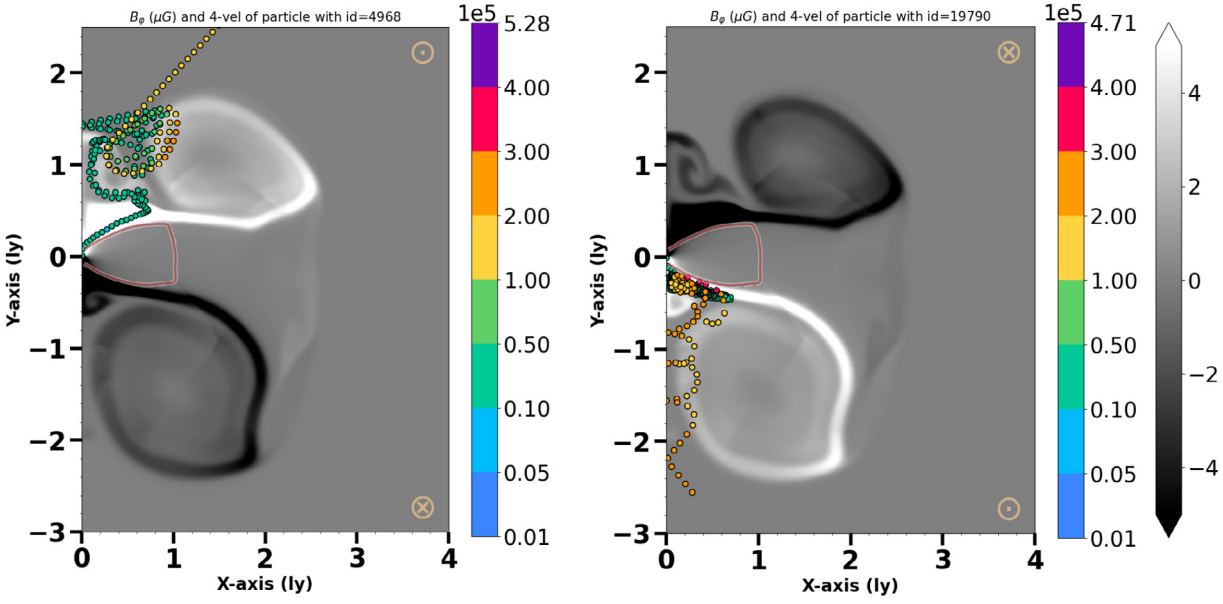

Fig. 4. Trajectories of protons accelerating in converging flows. In each panel bold dots show the positions of the proton at the set of consecutive time moments, the color of dots indicate the protons's 4-velocity according the colorbar on the right. The trajectories are superimposed onto a gray-color map of the PWN's azimuthal magnetic field, thin red contour shows the approximate position of the pulsar wind termination shock.

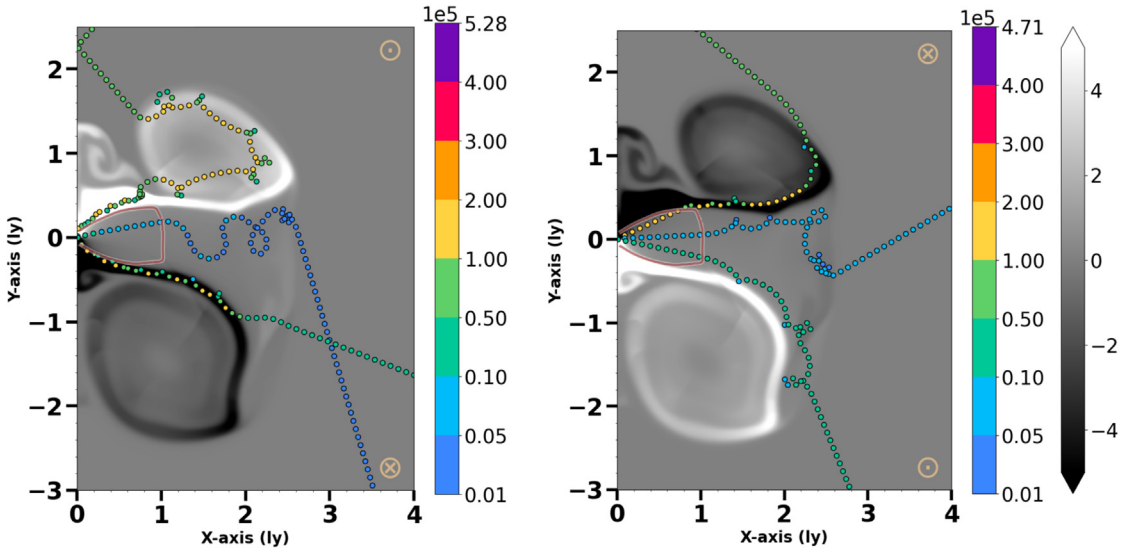

Fig. 6. Trajectories of three test particle protons in pulsar wind nebulae of the same structure but with opposite magnetic field polarity in the windward hemisphere. In each panel bold dots show the positions of the proton at the set of consecutive time moments, the color of dots indicate the protons's 4-velocity according the colorbar on the right. The trajectories are superimposed onto a gray-color map of the PWN's azimuthal magnetic field, thin red contour shows the approximate position of the pulsar wind termination shock.

hemisphere of the neutron star-pulsar). Fig. 6 illustrates that non-thermal protons injected at the same location as the pulsar wind and pre-accelerated to the Lorentz factor of $\sim 10^4$ can, in principle, reach any place in the nebula (at any polarity of its hemispheres). Accordingly, such protons can use any of the nebula's structures for their acceleration. To investigate in what structures and to what energies protons could be accelerated most effectively, we injected a population of test-particle protons into the model nebula and followed their evolution in space and energies.

The result of the modeling is in Fig. 7. It describes the population of high-energy non-thermal protons 9 years after their injection into the nebula. In this simulation, a population of $1.5 \cdot 10^6$ protons is injected into the nebula with a frozen pattern of MHD flows. The monoenergetic particles with Lorentz factor of $5 \cdot 10^4$ are injected uniformly, isotropically, and into all regions of the nebula at once. As can be seen in the figure, the nebula can accelerate protons to Lorentz factors above $\sim 5 \cdot 10^5$. The particles leaving the double-torus clearly tend to gather into three distinct populations. The most energetic of them

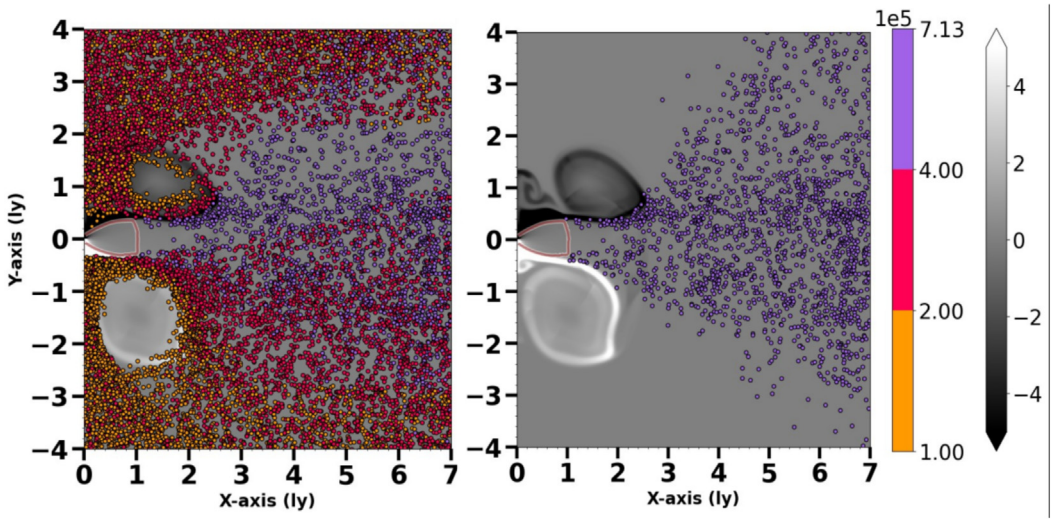

Fig. 7. Left panel: A snapshot of spatial distribution of high-energy non-thermal protons 9 years after their injection into the double-torus nebula. Each proton is marked with a bold dot, the color of which indicates the particle's 4-velocity according the colorbar on the right. The dots are superimposed on the gray-color map of the magnetic field of the nebula. The gray-color bar is in μGauss; its scale is adjusted to highlight the structure of MHD flows, so that its limits do not reflect the maximum and minimum values of the magnetic field in the model nebula. Right panel: A snapshot of angular distribution of the most energetic protons leaving the double-torus.

($\gamma > 4 \cdot 10^5$) has a very narrow angular distribution; its particles leave the double-torus predominantly along its equatorial plane, within an angular sector of $\pm 30^\circ$ around it. Protons from this population were first accelerated in the circulation vortex, and then further increased their energy in the relativistic narrow-channel flow running parallel to the equator. Two other populations have less anisotropic angular distributions. Protons in the second population, enclosing particles with Lorentz factors $\gamma \sim (2\text{–}4) \cdot 10^5$, accelerate predominantly in the windward hemisphere and leave the double-torus mainly in the windward direction. Protons in the third population with Lorentz factors $\gamma \sim (1\text{–}2) \cdot 10^5$, accelerate predominantly in the leeward hemisphere and leave it mainly in the leeward direction.

Our modeling of RMHD flows in a double torus PWNe is performed under imposed axial symmetry and thus produces two-dimensional fields. A note of caution is in order here. It concerns the constraints on the motions of CR particles that are imposed by the presence of one ignorable spatial coordinate. As shown in Jones et al., 1998, this may suppress CR particle diffusion across the local field lines. Full 3D modeling of nebulae at a resolution appropriate for modeling the propagation of cosmic ray particles is not feasible yet. A comparison of large-scale 2D and 3D simulations of the diffusive shock acceleration, performed for several magnetic field inclination angles, showed that the 2D results reproduce the 3D results quite adequately (Caprioli and Spitkovsky, 2014). Considering the fairly regular magnetic field geometry in the Vela PWN, as inferred from the observations of its radio and X-ray polarization, one can expect that the 2D model presented here is quite good; future 3D models are needed to verify the results.

Very high energy gamma-ray emission in the TeV regime is detected from the Vela PWN region (Aharonian et al., 2006; Abdalla et al., 2019). Most of the TeV radiation comes from the extended *X-ray cocoon,* the relic compact nebula swept away by the reverse shock. This radiation can be explained by a leptonic scenario in which relic electrons and positrons were accelerated to 100 TeV at the wind termination surface in the original Vela PWN that existed before the passage of the reverse shock (see e.g. Chevalier and Reynolds, 2011; Slane et al., 2018). Interpreting the TeV data, Abdalla et al., 2019 derived the energy density of TeV electrons and magnetic fields to be $\sim 10^{-12}$ erg cm^{-3}. The authors pointed out that such an energy density is not enough to ensure pressure balance in the cocoon, and some other dominant pressure component is required. The latter could possibly be provided either by mixing of the SN ejecta with the relic PWN (Slane et al., 2018) or by relativistic ions accelerated in the PWN. The mechanism discussed above could provide such a pressure component if a few percent of the pulsar's spin-down luminosity were transferred to relativistic ions, which would then be transported into the cocoon by advection or diffusion. The gamma-ray luminosity produced by hadronic interactions of the accelerated ions is difficult to disentangle in the Vela case. The cooling time of protons in the tenuous gas inside the Vela SNR is likely above

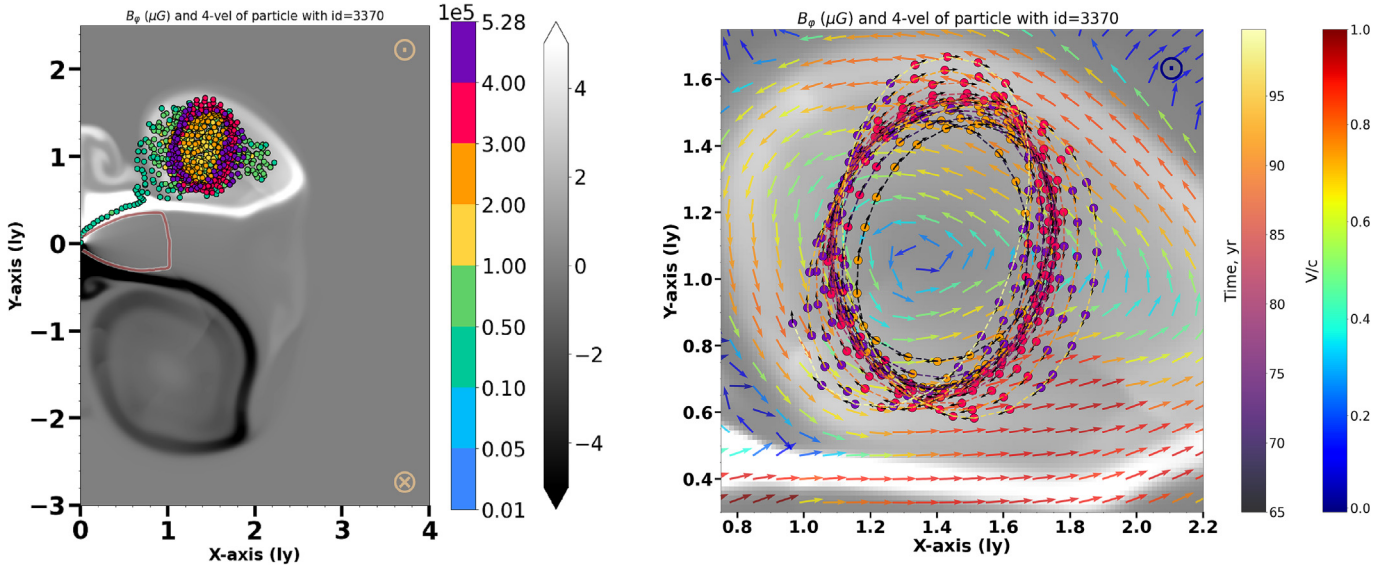

Fig. 8. An example of the trajectory of a proton test particle accelerating in the windward circulation vortex of a double X-ray torus nebula. On the left is a general view of the trajectory, on the right is a close-up of a fragment of this trajectory during the acceleration stage. Left: bold dots show the positions of the proton at the set of consecutive time moments, the color of dots indicate the proton's 4-velocity according the colorbar on the right. The trajectories are superimposed onto a gray-color map of the PWN's azimuthal magnetic field, thin red contour shows the approximate position of the pulsar wind termination shock. Right: the trajectory is shown simultaneously by (i) the color dots that show the positions of proton at the set of the consecutive moments of time, where the color shows the magnitude of the proton's 4-velocity and black arrows its direction and (ii) the dashed lines along the trajectory whose color shows the time since the proton's injection (colorbar marked 'Time, yr'). Color arrows show the magnitude and direction of the simulated RMHD flows' velocity (rightmost colorbar marked 'V/c').

10^{15} s, while the time limited by the age of the system accelerating the ions in our case is below 10^{12} s. This limits the luminosity of multi TeV hadronic emission in the Vela-X's X-ray cocoon to be below 10^{32} erg s^{-1}.

The hadronic emission may be expected in the case of Vela-type candidate source G63.7 + 1.1 where the likely presence of dense molecular environment was revealed from CO observations (see e.g. Matheson et al., 2016; Zhou et al., 2023). Recent analysis of the Fermi Observatory gamma-ray data and IceCube neutrino fluxes reported a possible source of hadronic emission associated with G63.7 + 1.1 (Ji et al., 2025). If confirmed with TeV observations, the source may provide the observational case to test the model we discussed above.

5. Conclusions

By direct numerical modeling we show that pulsar wind nebulae with a double-torus X-ray morphology can accelerate protons to energies of hundreds of TeV. The nebulae retain this ability as long as they maintain the MHD flow structure characteristic of double-torus objects. The duration of such stage in the nebula can vary from a thousand to tens of thousands of years, depending on a combination of parameters of both the pulsar and the external matter in which the pulsar moves. The ability to continuously accelerate protons over long periods of time could put double-torus nebulae in line with other possible sources of cosmic ray protons with energies of hundreds of TeV.

We believe that the RMHD model of double-torus nebulae we have constructed adequately describes real objects since its X-ray synchrotron radiation reproduces well the observed X-ray morphology of the double-torus nebula Vela (see the model synchrotron images in Ponomaryov et al., 2023). The gyroradii of multi-TeV CR protons injected into the system are large enough to be resolved by the simulation grid. This allows us to study the propagation and acceleration of protons by direct numerical solving the equations of particle motion in the simulated electromagnetic fields of the model nebula. It is shown that sub-PeV protons can be confined and accelerated in regular shear flows, which underlie almost all large-scale structures characteristic of double-toroidal nebulae.

We used the Vela Nebula as a prototype for our simulations because its X-ray structure has been studied in detail by the Chandra X-ray telescope with its excellent angular resolution of $\sim 0.5''$. This allowed us to test our MHD model on observations of this very complex object, which exhibits many fine X-ray structures. The model passed this test successfully. The estimated age of Vela suggests that this particular nebula, located 300 pc from Earth, may be too young to contribute directly to the local CR fluxes. In fact, its possible contribution depends sensitively on the model of local propagation of CRs. Currently, a few Vela-type PWNe is known in the Galaxy. The Boomerang nebula powered by a very energetic pulsar PSR J2229 + 6114 (Kothes et al., 2006), the PWN in G63.7 + 1.1 located in a dense environment, and the nebula powered by energetic pulsar PSR J2022 + 3842 in SNR G76.9 + 1.0 (Matheson et al., 2016; Arzoumanian et al., 2011) are among of the most interesting Vela-type candidates.

Declaration of Competing Interest

The authors declare that they have no known competing financial interests or personal relationships that could have appeared to influence the work reported in this paper.

Acknowledgments

We thank two reviewers for carefully reading this paper and for reports that helped us clarify our results. 3D RMHD modeling of the anisotropic pulsar wind nebulae by A.M.B. and A.N.F. was supported by the RSF grant 25–72-20007. The double-torus PWNe model setup and statistical analysis of accelerated protons by K.P.L. was supported by the baseline project FFUG-2024–0002 at the Ioffe Institute. Particles and antiparticles acceleration simulations by A.E.P. were supported by the Foundation for the Advancement of Theoretical Physics and Mathematics "BASIS". Some of the modeling was performed using the resources of the supercomputer center of St. Petersburg Polytechnic University, http://scc.spbstu.ru.

Appendix A. RMHD model

Modeling of high energy protons acceleration employs the RMHD-PIC approach on the base of the *Relativistic MHD module* and the *Cosmic Ray particle module* of the open-source code PLUTO (Mignone et al., 2007; Mignone et al., 2018).

The calculations were performed in the reference frame associated with the pulsar. Before inflating the nebula, a uniform directed flow of the external matter was initiated in the entire computation domain (except for a small area of radius r_{in} around the pulsar). The flow had fixed pressure, density, and velocity, and was directed along the polar axis of the nebula. After the initiation of the external flow, the pulsar wind was injected from a small area of radius r_{in} into the computation domain. The wind model is described in the Appendix B.

The numerical simulations are performed on a uniform 2D Cartesian grid with the pulsar at the origin. The pulsar's rotation axis is assumed to be parallel to the direction of the external flow going in the negative direction of the Y axis. The Mach number of the external flow is assumed to be $M = 1.3$, as in Vela (Chevalier and Reynolds, 2011). The simulation domain $x_{min} = 0 < x < x_{max} = 7, \quad y_{min} = -5 < y < y_{max} = 5$ has $N_x = 500$ nodes along the X-axis and $N_y = 700$ nodes along the Y-axis. The grid resolution $\Delta x = \Delta y \approx 0.014$ ly

(all lengths are given in light years). The boundary conditions in the simulation are free outflow for the background RMHD plasma and free escape for non-thermal particles. The exception is the boundary $x = 0$, at which the axisymmetric condition for fluid modeling is employed. All non-thermal particles reaching this boundary are reflected back into the computation domain.

Following a typical approach (see e.g., p.1.2.1 of Del Zanna and Olmi, 2017), the equation of state of an ideal plasma with a constant adiabatic index 4/3 is adopted both for the nebular and external flows. We also neglected the radiative losses in simulations of the PWN's structure.

Appendix B. Model of the pulsar wind

We use the pulsar wind model of Porth et al. (2014) that is widely applied for simulations of PWNe in the literature.

The free parameters of this model are: the inclination of the pulsar α, its spin-down luminosity L, the initial Lorentz factor Γ and the initial magnetization σ_0 of the pulsar wind. The inclination is defined as the tilt angle between the pulsar's spin and magnetic axes. The initially cold pulsar wind is latitudinally anisotropic. It carries the total energy flux density

$$f_{tot}(r,\theta) = \frac{L}{L_0}\frac{1}{r^2}\cdot\left(\sin^2\theta + \varepsilon\right). \quad (1)$$

that depends on the colatitude θ and the radial coordinate r. Here $L_0 = 4\pi(2/3+\varepsilon)$ is just a normalization constant, and $\varepsilon = 0.02$ is introduced to evade the energy flux vanishing at the poles.

The total energy flux is divided into magnetic and kinetic fractions, $f_{tot} = f_m + f_k$:

$$f_m(r,\theta) = \frac{\sigma(\theta)\cdot f_{tot}(r,\theta)}{1+\sigma(\theta)}; \quad f_k(r,\theta) = \frac{f_{tot}(r,\theta)}{1+\sigma(\theta)}. \quad (2)$$

and the ratio of these fractions determines the wind magnetization $\sigma = f_m/f_k$ (upstream of the termination shock) at a given colatitude:

$$\sigma(\theta) = \frac{\tilde{\sigma}(\theta)\cdot\chi_\alpha(\theta)}{1+\tilde{\sigma}(\theta)\cdot(1-\chi_\alpha(\theta))}. \quad (3)$$

The purely toroidal magnetic field of the wind is frozen into plasma. It must vanish at the poles and change sign at the plane of the pulsar's rotational equator, what is parameterized by the functions $\tilde{\sigma}$ and χ in Eq. 3:

$$\tilde{\sigma}(\theta) = \sigma_0\cdot\min\left\{1,\ \theta^2/\theta_0^2,\ (\pi-\theta)^2/\theta_0^2\right\}; \quad (4)$$

$$\chi_\alpha(\theta) = \begin{cases} (2\phi_a(\theta)/\pi - 1)^2 & \text{if } |\pi/2-\theta| < \alpha \\ 1 & \text{otherwise} \end{cases}, \quad (5)$$

where $\phi_\alpha(\theta) = \arccos(-\cot(\theta)\cot(\alpha))$. The parameter $\theta_0 = 10^\circ$, and σ_0 is an initial magnetization of the pulsar wind at the pulsar's light cylinder. Due to the sign change, in the equatorial sector of the angular extent of $\pm\alpha$ the wind carries stripes of alternating magnetic polarity, that are supposed to annihilate at the termination shock or on the way to it (Lyubarsky, 2003; Komissarov, 2013; Cerutti et al., 2020). Hence, within this sector the magnetic field should dissipate, as described by Eqs. (3)–(5).

The magnetic field and density of the pulsar wind are calculated using Eq. (2) as follows:

$$B_{pw}(r,\theta) = \pm\sqrt{4\pi f_m(r,\theta)/c}, \quad \rho_{pw}(r,\theta) = \frac{f_k(r,\theta)}{\Gamma_w^2 c^3}. \quad (6)$$

The velocity of the wind is directed radially outwards with the magnitude

$$u_{pw}/c = \sqrt{1-\Gamma_w^{-2}}. \quad (7)$$

where c is the light velocity. On the inner boundary of the wind, we use the equation of state for an ideal relativistic plasma to calculate its pressure. Radial coordinate and colatitude are expressed as follows:

$$r = \sqrt{x^2+y^2}; \quad \theta = \arccos\left(y/\sqrt{x^2+y^2}\right) \quad (8)$$

Because the production of double-torus structures similar to one in the Vela PWN requires high inclination and low initial magnetization, in the presented setup we use $\alpha = 80^\circ$ and $\sigma_0 = 0.1$. We use the spin-down luminosity of the Vela pulsar $L = 6.9\times10^{36}\,\mathrm{erg\,s^{-1}}$.

Appendix C. Modeling of particle propagation

In our RMHD-PIC modeling, the evolution of MHD flows in the model nebula is followed until the nebula reaches a stage of self-similar evolution. With the chosen parameters, this takes about 6–8 years for the nebula. To save numerical resources, we freeze the structure of MHD flows in the nebula when the latter reaches the age of 10 years, and then inject non-thermal test-particle protons into the nebula. So from the point of view of accelerating protons, the MHD structure of the nebula begins to look stationary (but not static!): in each cell of the model nebula, the magnitude of the local field, as well as the direction and magnitude of the local velocity, did not change during the entire acceleration process. The evolution of non-thermal protons in the MHD flows of a background nebular plasma is followed using the conventional particle-in-cell techniques implemented in the *Cosmic Ray* module of code *PLUTO* (Mignone et al., 2018). The population of mono-energetic non-thermal protons is injected at the same location as the pulsar wind. The injected protons are treated as test particles. All injected protons have an energy of $\sim 10^4$ GeV; the directions of their velocities are random, with a uniform angular distribution.

The acceleration time of very high energy (VHE) protons in our calculations is about 20 years. Using the stationary structure of MHD flows for particle acceleration is justified if their dynamic time is longer than the acceleration time. Our simulations of double-torus nebulae show that all their large-scale MHD structures (two narrow-

channel flows, two circulation vortices, etc.), essential for accelerating VHE protons, are very regular (although some smaller-scale structures may exhibit minor evolution on decadal time scales). Available observations of the Vela Nebula (Kargaltsev et al., 2015) are not in conflict with this assumption. In our MHD model, protons are accelerated via a non-resonant Fermi-type mechanism in shearing flows. This mechanism is not very sensitive to small scale transient structures.

References

Aharonian, F., Akhperjanian, A.G., Bazer-Bachi, A.R., et al., 2006. First detection of a VHE gamma-ray spectral maximum from a cosmic source: HESS discovery of the Vela X nebula. Astron. Astrophys. 448 (2), L43–L47. https://doi.org/10.1051/0004-6361:200600014, arXiv:astro-ph/0601575.

Amato, E., 2014. The origin of galactic cosmic rays. Int. J. Modern Phys. D 23 (7), 1430013. https://doi.org/10.1142/S0218271814300134, arXiv:1406.7714.

Amato, E., Arons, J., 2006. Heating and nonthermal particle acceleration in relativistic, transverse magnetosonic shock waves in proton-electron-positron plasmas. ApJ 653 (1), 325–338. https://doi.org/10.1086/508050, arXiv:astro-ph/0609034.

Amato, E., & Olmi, B. (2021). The Crab Pulsar and Nebula as Seen in Gamma-Rays. Universe, 7(11), 448. doi:10.3390/universe7110448. arXiv:2111.07712.

Arons, J., 2003. Magnetars in the metagalaxy: an origin for ultra-high-energy cosmic rays in the nearby universe. ApJ 589 (2), 871–892. https://doi.org/10.1086/374776, arXiv:astro-ph/0208444.

Arons, J., 2012. Pulsar wind nebulae as cosmic pevatrons: a current sheet's tale. Space Sci. Rev. 173 (1–4), 341–367. https://doi.org/10.1007/s11214-012-9885-1, arXiv:1208.5787.

Arzoumanian, Z., Gotthelf, E.V., Ransom, S.M., Safi-Harb, S., Kothes, R., Landecker, T.L., 2011. Discovery of an energetic pulsar associated with SNR G76.9+1.0. ApJ 739 (1), 39. https://doi.org/10.1088/0004-637X/739/1/39, arXiv:1105.3185.

Bednarek, W., Bartosik, M., 2004. Cosmic rays from galactic pulsars. Astron. Astrophys. 423, 405–413. https://doi.org/10.1051/0004-6361:20047005, arXiv:astro-ph/0405310.

Bell, A.R., 1992. Cosmic ray acceleration in pulsar-driven supernova remnants. MNRAS 257, 493–500. https://doi.org/10.1093/mnras/257.3.493.

Bell, A.R., Lucek, S.G., 1996. Cosmic ray acceleration in pulsar-driven supernova remnants: the effect of scattering. MNRAS 283 (3), 1083–1088. https://doi.org/10.1093/mnras/283.3.1083.

Berezhko, E.G., 1994. Generation of ultrahigh-energy cosmic rays in the surroundings of pulsars. Astron. Lett. 20 (1), 75–79.

Blandford, R., Eichler, D., 1987. Particle acceleration at astrophysical shocks: a theory of cosmic ray origin. Phys. Rep. 154, 1–75.

Bykov, A.M., Amato, E., Petrov, A.E., Krassilchtchikov, A.M., Levenfish, K.P., 2017. Pulsar wind nebulae with bow shocks: non-thermal radiation and cosmic ray leptons. Space Sci. Rev. 207, 235–290. https://doi.org/10.1007/s11214-017-0371-7, arXiv:1705.00950.

Bykov, A.M., Ellison, D.C., Marcowith, A., Osipov, S.M., 2018. Cosmic ray production in supernovae. Space Sci. Rev. 214 (1), 41. https://doi.org/10.1007/s11214-018-0479-4, arXiv:1801.08890.

Bykov, A.M., Petrov, A.E., Krassilchtchikov, A.M., Levenfish, K.P., Osipov, S.M., Pavlov, G.G., 2019. GeV-TeV cosmic-ray leptons in the solar system from the bow shock wind nebula of the nearest millisecond pulsar J0437–4715. ApJ Lett. 876 (1), L8. https://doi.org/10.3847/2041-8213/ab1922, arXiv:1904.09430.

Bykov, A.M., Petrov, A.E., Ponomaryov, G.A., Levenfish, K.P., Falanga, M., 2024. PeV proton acceleration in gamma-ray binaries. Adv. Space Res. 74 (9), 4276–4289. https://doi.org/10.1016/j.asr.2024.01.021, arXiv:2401.06271.

Cao, Z., Aharonian, F., An, Q., et al., 2024. The First LHAASO catalog of gamma-ray sources. Astrophys. J. Suppl. Ser. 271 (1), 25. https://doi.org/10.3847/1538-4365/acfd29, arXiv:2305.17030.

Caprioli, D., Spitkovsky, A., 2014. Simulations of ion acceleration at non-relativistic shocks. I. Acceleration Efficiency. ApJ 783 (2), 91. https://doi.org/10.1088/0004-637X/783/2/91, arXiv:1310.2943.

Cerutti, B., Philippov, A.A., Dubus, G., 2020. Dissipation of the striped pulsar wind and non-thermal particle acceleration: 3D PIC simulations. Astron. Astrophys. 642, A204. https://doi.org/10.1051/0004-6361/202038618, arXiv:2008.11462.

Chevalier, R.A., Reynolds, S.P., 2011. Pulsar Wind Nebulae with Thick Toroidal Structure. ApJ Lett. 740 (1), L26. https://doi.org/10.1088/2041-8205/740/1/L26, arXiv:1109.1752.

Del Zanna, L., Amato, E., Bucciantini, N., 2004. Axially symmetric relativistic MHD simulations of Pulsar Wind Nebulae in Supernova Remnants. On the origin of torus and jet-like features. Astron. Astrophys. 421, 1063–1073. https://doi.org/10.1051/0004-6361:20035936, arXiv:astro-ph/0404355.

Del Zanna, L., & Olmi, B. (2017). Multidimensional Relativistic MHD Simulations of Pulsar Wind Nebulae: Dynamics and Emission. In D.F. Torres (Ed.), Modelling Pulsar Wind Nebulae (p. 215). volume 446 of Astrophysics and Space Science Library. doi:10.1007/978-3-319-63031-1_10. arXiv:1703.10442.

Fateeva, S.S., Levenfish, K.P., Ponomaryov, G.A., Petrov, A.E., Fursov, A.N., 2023. On the nature of the bar-shaped x-ray feature in the lee jet of the vela pulsar wind nebula. Astron. Lett. 49 (2), 56–64. https://doi.org/10.1134/S1063773723020020.

Guépin, C., Cerutti, B., Kotera, K., 2020. Proton acceleration in pulsar magnetospheres. Astron. Astrophys. 635, A138. https://doi.org/10.1051/0004-6361/201936816, arXiv:1910.11387.

Collaboration, H.E.S.S., Abdalla, H., Abramowski, A., et al., 2018. The population of TeV pulsar wind nebulae in the H.E.S.S. Galactic Plane Survey. Astron. Astrophys. 612, A2. https://doi.org/10.1051/0004-6361/201629377, arXiv:1702.08280.

Collaboration, H.E.S.S., Abdalla, H., Aharonian, F., et al., 2019. H.E.S.S. and Suzaku observations of the Vela X pulsar wind nebula. Astron. Astrophys. 627, A100. https://doi.org/10.1051/0004-6361/201935458, arXiv:1905.07975.

Helfand, D.J., Gotthelf, E.V., Halpern, J.P., 2001. Vela Pulsar and Its Synchrotron Nebula. ApJ 556 (1), 380–391. https://doi.org/10.1086/321533, arXiv:astro-ph/0007310.

Ji, S., Wang, Z., Zheng, D., & Zheng, J. (2025). Possible Neutrino Emission from the Pulsar Wind Nebula G63.7+1.1. arXiv e-prints, (p. arXiv:2507.19724). doi:10.48550/arXiv.2507.19724. arXiv:2507.19724.

Jones, F.C., Jokipii, J.R., Baring, M.G., 1998. Charged-particle motion in electromagnetic fields having at least one ignorable spatial coordinate. ApJ 509 (1), 238–243. https://doi.org/10.1086/306480, arXiv:astro-ph/9808103.

Kargaltsev, O., Cerutti, B., Lyubarsky, Y., Striani, E., 2015. Pulsar-wind nebulae. recent progress in observations and theory. Space Sci. Rev. 191 (1–4), 391–439. https://doi.org/10.1007/s11214-015-0171-x, arXiv:1507.03662.

Komissarov, S.S., 2013. Magnetic dissipation in the Crab nebula. MNRAS 428 (3), 2459–2466. https://doi.org/10.1093/mnras/sts214, arXiv:1207.3192.

Komissarov, S.S., Lyubarsky, Y.E., 2004. Synchrotron nebulae created by anisotropic magnetized pulsar winds. MNRAS 349 (3), 779–792. https://doi.org/10.1111/j.1365-2966.2004.07597.x.

Kotera, K., Amato, E., Blasi, P., 2015. The fate of ultrahigh energy nuclei in the immediate environment of young fast-rotating pulsars. J. Cosmol. Astropart. Phys. 2015 (8). https://doi.org/10.1088/1475-7516/2015/08/026, 026–026. arXiv:1503.07907.

Kothes, R., Reich, W., Uyanıker, B., 2006. The Boomerang PWN G106.6+2.9 and the magnetic field structure in pulsar wind nebulae. ApJ 638 (1), 225–233. https://doi.org/10.1086/498666.

Levenfish, K.P., Ponomaryov, G.A., & Fursov, A.N. (2025). accepted to Pisma v Astron. Zh., 51(3).

Levenfish, K.P., Ponomaryov, G.A., Petrov, A.E., Bykov, A.M., & Krassilchtchikov, A.M. (2021). Slow motion pulsar wind nebulae. In Journal of Physics Conference Series (p. 012020). IOP volume 2103 of Journal of Physics Conference Series. doi:10.1088/1742-6596/2103/1/012020.

Collaboration, L.H.A.A.S.O., Cao, Z., Aharonian, F., et al., 2021. Peta-electron volt gamma-ray emission from the Crab Nebula. Science 373, 425–430. https://doi.org/10.1126/science.abg5137, arXiv:2111.06545.

Lyubarsky, Y.E., 2003. The termination shock in a striped pulsar wind. MNRAS 345 (1), 153–160. https://doi.org/10.1046/j.1365-8711.2003.06927.x, arXiv:astro-ph/0306435.

Malkov, M.A., Drury, L., 2001. Nonlinear theory of diffusive acceleration of particles by shock waves. Rep. Prog. Phys. 64, 429–481.

Malkov, M.A., Moskalenko, I.V., 2021. The TeV Cosmic-Ray Bump: A Message from the Epsilon Indi or Epsilon Eridani Star?. ApJ 911 (2), 151. https://doi.org/10.3847/1538-4357/abe855, arXiv:2010.02826.

Marcowith, A., Ferrand, G., Grech, M., Meliani, Z., Plotnikov, I., Walder, R., 2020. Multi-scale simulations of particle acceleration in astrophysical systems. Living Rev. Comput. Astrophys. 6 (1), 1. https://doi.org/10.1007/s41115-020-0007-6, arXiv:2002.09411.

Matheson, H., Safi-Harb, S., Kothes, R., 2016. XMM-Newton and Chandra observations of the filled-center supernova remnant G63.7 +1.1. ApJ 825 (2), 134. https://doi.org/10.3847/0004-637X/825/2/134.

Mattana, F., Götz, D., Terrier, R., Bouchet, L., Ponti, G., Falanga, M., Renaud, M., Caballero, I., Soldi, S., Zurita Heras, J.A., Schanne, S., 2011. Extended hard x-ray emission from the vela pulsar wind nebula. ApJ Lett. 743 (1), L18. https://doi.org/10.1088/2041-8205/743/1/L18, arXiv:1111.2163.

Mignone, A., Bodo, G., Massaglia, S., Matsakos, T., Tesileanu, O., Zanni, C., Ferrari, A., 2007. PLUTO: a numerical code for computational astrophysics. Astrophys. J. Suppl. Ser. 170 (1), 228–242. https://doi.org/10.1086/513316, arXiv:astro-ph/0701854.

Mignone, A., Bodo, G., Vaidya, B., Mattia, G., 2018. A Particle Module for the PLUTO Code. I. An Implementation of the MHD-PIC Equations. ApJ 859 (1), 13. https://doi.org/10.3847/1538-4357/aabccd, arXiv:1804.01946.

Pavlov, G.G., Kargaltsev, O.Y., Sanwal, D., Garmire, G.P., 2001. Variability of the Vela Pulsar Wind Nebula Observed with Chandra. ApJ Lett. 554 (2), L189–L192. https://doi.org/10.1086/321721, arXiv:astro-ph/0104264.

Petrov, A.E., Levenfish, K.P., Ponomaryov, G.A., 2023. Reverberation of the vela pulsar wind nebula. Astron. Lett. 49 (12), 777–786. https://doi.org/10.1134/S106377372312006X.

Philippov, A.A., Spitkovsky, A., 2018. Ab-initio pulsar magnetosphere: particle acceleration in oblique rotators and high-energy emission modeling. ApJ 855 (2), 94. https://doi.org/10.3847/1538-4357/aaabbc, arXiv:1707.04323.

Ponomaryov, G.A., Fursov, A.N., Fateeva, S.S., Levenfish, K.P., Petrov, A.E., Krassilchtchikov, A.M., 2023. On the origin of knots in the vela nebula. Astron. Lett. 49 (2), 65–79. https://doi.org/10.1134/S1063773723020032.

Ponomaryov, G.A., Levenfish, K.P., & Petrov, A.E. (2019). Two tori of the Vela pulsar wind nebula. In Journal of Physics Conference Series (p. 022027). IOP volume 1400 of Journal of Physics Conference Series. doi:10.1088/1742-6596/1400/2/022027.

Ponomaryov, G.A., Levenfish, K.P., & Petrov, A.E. (2021). Jet and counter-jet in transonic pulsar wind nebulae. In Journal of Physics Conference Series (p. 012021). IOP volume 2103 of Journal of Physics Conference Series. doi:10.1088/1742-6596/2103/1/012021.

Ponomaryov, G.A., Levenfish, K.P., Petrov, A.E., Kropotina, Y.A., 2020. On stability of toroidal structures in two-tori pulsar wind nebulae. In: In Journal of Physics Conference Series (p. 012022). volume 1697 of Journal of Physics Conference Series. https://doi.org/10.1088/1742-6596/1697/1/012022.

Porth, O., Komissarov, S.S., Keppens, R., 2014. Three-dimensional magnetohydrodynamic simulations of the Crab nebula. MNRAS 438 (1), 278–306. https://doi.org/10.1093/mnras/stt2176, arXiv:1310.2531.

Reynolds, S.P., Pavlov, G.G., Kargaltsev, O., Klingler, N., Renaud, M., Mereghetti, S., 2017. Pulsar-wind nebulae and magnetar outflows: observations at radio, x-ray, and gamma-ray wavelengths. Space Sci. Rev. 207 (1–4), 175–234. https://doi.org/10.1007/s11214-017-0356-6, arXiv:1705.08897.

Slane, P., Lovchinsky, I., Kolb, C., Snowden, S.L., Temim, T., Blondin, J., Bocchino, F., Miceli, M., Chevalier, R.A., Hughes, J.P., Patnaude, D.J., Gaetz, T., 2018. Investigating the Structure of Vela X. ApJ 865 (2), 86. https://doi.org/10.3847/1538-4357/aada12, arXiv:1808.03878.

van der Swaluw, E., Achterberg, A., Gallant, Y.A., Downes, T.P., Keppens, R., 2003. Interaction of high-velocity pulsars with supernova remnant shells. Astron. Astrophys. 397, 913–920. https://doi.org/10.1051/0004-6361:20021488, arXiv:astro-ph/0202232.

Weisskopf, M.C., Hester, J.J., Tennant, A.F., Elsner, R.F., Schulz, N.S., Marshall, H.L., Karovska, M., Nichols, J.S., Swartz, D.A., Kolodziejczak, J.J., O'Dell, S.L., 2000. Discovery of spatial and spectral structure in the x-ray emission from the crab nebula. ApJ Lett. 536 (2), L81–L84. https://doi.org/10.1086/312733, arXiv:astro-ph/0003216.

Xie, F., Di Marco, A., La Monaca, F., et al., 2022. Vela pulsar wind nebula X-rays are polarized to near the synchrotron limit. Nature 612 (7941), 658–660. https://doi.org/10.1038/s41586-022-05476-5, arXiv:2303.12437.

Zhou, X., Su, Y., Yang, J., Chen, X., Sun, Y., Jiang, Z., Wang, M., Wang, H., Zhang, S., Xu, Y., Yan, Q., Yuan, L., Chen, Z., Ao, Y., Ma, Y., 2023. A systematic study of associations between supernova remnants and molecular clouds. Astrophys. J. Suppl. Ser. 268 (2), 61. https://doi.org/10.3847/1538-4365/acee7f, arXiv:2308.03484.